Ultrafast and continuous synthesis of crystalline ferrite nanoparticles in supercritical ethanol

Oana Pascu, Samuel Marre, Cyril Aymonier, Anna Roig

PAPER

Ultrafast and continuous synthesis of crystalline ferrite nanoparticles in supercritical ethanol

Oana Pascu,[a] Samuel Marre,[bc] Cyril Aymonier*[bc] and Anna Roig*[a]

Magnetic nanoparticles (NPs) are of increasing interest in various industrially relevant products. For these, the development of greener and faster approaches facilitating scaling-up production is of paramount importance. Here, we report a novel, green and potentially scalable approach for the continuous and ultrafast (90 s) synthesis of superparamagnetic ferrite NPs ($MnFe_2O_4$, Fe_3O_4) in supercritical ethanol (scEtOH) at a fairly moderate temperature (260 °C). ScEtOH exhibits numerous advantages such as its production from bio-resources, its lack of toxicity and its relatively low supercritical coordinates (p_c = 6.39 MPa and T_c = 243 °C), being therefore appropriate for the development of sustainable technologies. The present study is completed by the investigation of both *in situ* and *ex situ* NP surface functionalization. The as-obtained nanoparticles present good crystallinity, sizes below 8 nm, superparamagnetic behavior at room temperature and high saturation magnetization. Moreover, depending on the capping strategy, the ferrite NPs present extended (for *in situ* coated NPs) or short-term (for *ex situ* coated NPs) colloidal stability.

Introduction

One of the current major challenges in materials science is the design of functional nanostructures combining superior properties with reliable material processing technologies. Among all types of nanoparticles (NPs), magnetic ones are of enormous significance in various industrially relevant products such as magnetic resonance imaging contrast agents, drug delivery carriers, immunoassays, ultra-high density storage memories, magneto-photonic components, magnetic catalysts, environmental remediators or sensors.[1–11] For the implementation of magnetic NPs in these applications, the development of greener and faster approaches allowing scale-up production is of paramount importance. Several strategies directed towards cheaper and environmentally friendly scalable technologies[12–15] are currently being investigated. Different fronts covered are: the use of environmentally benign solvents (*e.g.* water, supercritical fluids, ionic liquids), the use of cheap and non-toxic chemicals, the exploitation of alternative energy sources (*e.g.* microwave, solar) or the design of fast and high yield processes. In this scenario, the utilization of supercritical fluids is worth considering.[16] Supercritical fluids provide homogeneous single phase reaction media combining the advantages of both liquids (density and solvation capabilities) and gases (high diffusivity, low viscosity and zero surface tension).[17–19] Moreover, their adjustable physical properties by slight variation of temperature and pressure and the increased overall reaction rate offer good conditions for nanomaterials synthesis, which has been reviewed several times over the past five years.[17–21] These reaction media have been used to synthesize various inorganic materials with controlled size, from the micrometer down to the nanometer scale.[18,20,22–24] Moreover, complex shapes and compositions have also been achieved.[25,26] The control of the chemical reaction, and therefore of the materials characteristics (size, morphology, structure, composition and architecture), is accomplished by choosing specific operating parameters among pressure, temperature, residence time, precursor nature and concentration. Additionally, the choice of the supercritical solvent is of primary importance. Reactions were reported in a large variety of solvents such as scH_2O,[27–30] $scCO_2$–alcohols,[26,31,32] scMeOH,[22] scEtOH,[23,33,34] sciPrOH,[24,35] alcohol–H_2O mixtures,[36–38] or alkanes.[39,40] To date, we have been able to identify only one work reporting the synthesis of magnetic ferrite NPs in scEtOH. The synthesis was performed in a batch mode with a reaction time of approximately 25 min at a relatively high temperature of 350 °C (100 °C above the critical temperature of EtOH, 243 °C).[23] As a solvent, ethanol exhibits great advantages over water or even methanol. In comparison with water, the supercritical coordinates of ethanol (p_c = 6.39 MPa and T_c = 243 °C) are much lower than those of water (p_c = 22.1 MPa and T_c = 374 °C), offering the opportunity to develop supercritical fluid based technology with lower energy consumption. In terms of toxicity, ethanol is much less harmful to humans[41] compared to methanol. Additionally, ethanol,

[a]*Institut de Ciència de Materials de Barcelona (ICMAB-CSIC), Campus UAB, E08193, Bellaterra, Spain. E-mail: roig@icmab.es*

[b]*CNRS, ICMCB, UPR 9048, F-33600 Pessac, France*

[c]*Univ. Bordeaux, ICMCB, UPR 9048, F-33600 Pessac, France. E-mail: aymonier@icmcb-bordeaux.cnrs.fr*

which can be obtained from bio-resources, is more appropriate for the development of sustainable technologies. Nanomaterials synthesized in scEtOH can also be easily recovered, while the solvent ethanol can be recycled by distillation and later reused.

Here, we report a novel, potentially scalable approach for the continuous and ultrafast (90 s) synthesis of superparamagnetic ferrite NPs ($MnFe_2O_4$, Fe_3O_4) in scEtOH at a fairly moderate temperature (260 °C). The study is completed by the investigation of both *in situ*[16,33] and e*x situ*[42] NP surface functionalization. The as-obtained NPs present good crystallinity, sizes below 8 nm and superparamagnetic behavior at room temperature. Moreover, depending on the considered capping strategy, the ferrite NPs present extended (for *in situ* coating nanoparticles) or short-term (for *ex situ* coating nanoparticles) colloidal stability.

Methodology

Chemicals

The chemicals were purchased from Sigma-Aldrich and used as received: iron(III) nitrate 9-hydrate ($Fe(NO_3)_3 \cdot 9H_2O$, >98%), iron(III) acetylacetonate ($Fe(acac)_3$, 97%), manganese(II) acetate tetrahydrate ($Mn(ac)_2 \cdot 4H_2O$, 99%), oleic acid (OAc, analytical standard), oleylamine (OAm, technical grade, 70%), and absolute ethanol.

Continuous synthesis in supercritical ethanol

The synthesis of ferrite NPs (Fe_3O_4, $MnFe_2O_4$) in a continuous system was partially adapted from a wet-chemical synthesis (thermal decomposition method).[12] Different strategies were evaluated: (i) the synthesis of iron oxide NPs, using an iron nitrate salt $Fe(NO_3)_3 \cdot 9H_2O$ (labeled A) and a metal precursor $Fe(acac)_3$ (labeled B), in the presence of surfactants (OAc and OAm) with a molar ratio [OAc : OAm : metal precursor (Fe^{3+})] of 3 : 3 : 1 (*in situ* functionalization) and (ii) the synthesis of $MnFe_2O_4$ NPs using $Mn(ac)_2 \cdot 4H_2O$ and $Fe(acac)_3$ (molar ratio 1 : 2) with *in situ* (labeled C) and *ex situ* (labeled D) functionalization (molar ratio [OAc : total metal precursors] of 3 : 1).

The NPs were prepared using a homemade continuous reactor setup. Fig. 1 shows a schematic representation of the system. The metal precursor in ethanol solution (S_1, concentration of 2×10^{-2} M) is injected with a high-pressure pump (HPP) at 20 MPa at room temperature and at a flow rate of 450 μL min^{-1} (Q_1) into the T-type mixing point and sequentially into the tubular reactor. A second ethanol solution containing the surfactant (S_2, concentration of 6×10^{-2} M) is injected by a second HPP under similar conditions as S_1 (pressure, flow rate) into the mixing point and then together with S_1 in the tubular reactor. The mixture was therefore pumped at a total flow rate of 900 μL min^{-1} (Q_2) through the heated tubular reactor. The reactor was heated (260 °C) with a silicon oil bath and magnetically stirred to ensure a homogeneous temperature, while the pressure was controlled with a back-pressure regulator downstream (20 MPa). The chemical reaction took place in a tubular reactor made of stainless steel (1 m long, internal diameter of 1.6 mm). The inlet flow rate (Q_2) was chosen to provide an optimal residence time of 90 s. The as-obtained NPs were recovered in liquid ethanol through the exit tube of the reactor at room temperature, where the reaction is quenched. The outlet solution was dark, containing a black precipitate responding to a magnet. The *in situ* functionalized NPs were separated from the outlet solution by adding extra ethanol (in 3× dilution) followed by centrifugation at 6500 rpm for 30 min. The supernatant was discharged and the precipitate was dried overnight and subsequently redispersed in 2 mL of hexane containing 10 μL of oleic acid. For the *ex situ* functionalization, the outlet solution was recovered in a flask containing a few μL of oleic acid, mixed for a few minutes and followed by a separation step by adding extra ethanol and centrifuging at 6500 rpm for 30 min. The as-separated black precipitate was dried and redispersed in 2 mL of hexane containing extra oleic acid (~10 μL). The colloidal dispersions were used for further characterization.

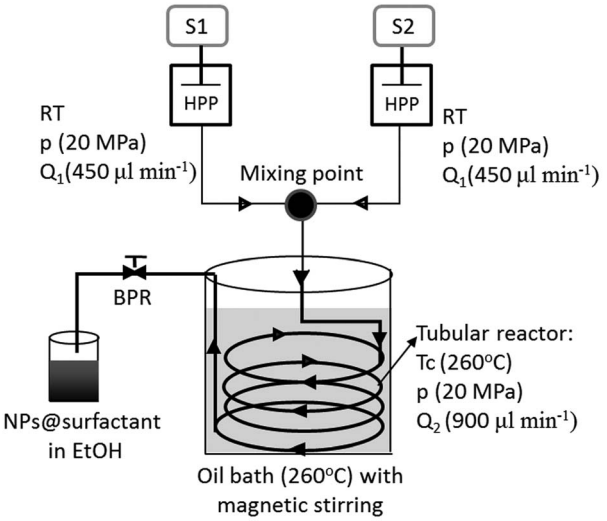

Fig. 1 The ICMCB continuous supercritical ethanol setup for the synthesis of ferrite nanoparticles.

Materials characterization

Morphological and structural characterizations were performed using transmission electron microscopy (TEM, HITACHI H7650) and X-ray powder diffraction (PANalytical X'Pert Pro with Cu $\lambda_{K\alpha}$ radiation). The TEM samples were prepared by depositing a drop of diluted hexane NP dispersion onto a copper–carbon grid and allowing the solvent to evaporate. The mean diameter and polydispersity of each system were determined by fitting a particle size histogram measured from TEM images by using the imageJ software to a Gaussian distribution (over 250 counts). The MAUD program (Materials Analysis Using Diffraction) with the MAUD refinement method was used to extract the unit cell lattice parameters. An experimental resolution function was obtained from the refinement of a quartz reference in order to take into account the instrumental

broadening. The weight percentage of surfactant on the NP surface was determined by thermogravimetry analysis (TGA). Solid samples (approx. 4 mg each) were characterized with a Pyris™ 1 TGA analyser (PerkinElmer) at a heating rate of 10 °C min^{-1} in a temperature range of 30–600 °C under a N_2 flux. The hydrodynamic diameter of NPs suspended in organic medium was measured with a Zetasizer Nano ZS from Malvern Instruments equipped with a He/Ne 633 nm laser. Special care was taken to check the DLS peak position and width, which appeared to be the same after three consecutive runs of 15 scans each. Magnetic characterization was performed with a superconductive quantum interference device (SQUID) magnetometer (Quantum Design MPMS5XL). The sample was prepared by using a gelatine capsule filled with compact cotton impregnated with 200 μL of hexane dispersion of NPs (equivalent to 2 mg of magnetic material plus surfactant). The magnetization values were reported per mass of ferrite by subtracting the mass of surfactant as measured in TGA experiments.

A redox titration was performed to evaluate the amount of Fe^{2+} and Fe^{3+} ions within the NPs. 1 mL of the colloidal dispersion was dissolved in HCl 37% v/v resulting in a yellow coloured solution (with Fe^{2+} and Fe^{3+} ions). A first addition of a $K_2Cr_2O_7$ (5 mM) oxidizing solution allows for proportioning the amount of Fe^{2+} ions in solution, by following their oxidation to Fe^{3+} (volume of Fe^{2+}: $V_{Fe^{2+}}$). This was indicated using a coloured indicator (sodium diphenylamine sulphonate) in the solution. The resulting solution containing only Fe^{3+} ions was thereafter entirely reduced to Fe^{2+} ions by adding a $SnCl_2$ reductive agent. Therefore, when $K_2Cr_2O_7$ was added for a second time, the total amount of iron was titrated (total volume of iron = V_{totFe}). The amount of Fe^{3+} could then be estimated by a simple subtraction $V_{Fe^{3+}} = V_{totFe} - V_{Fe^{2+}}$.

Results and discussion

We present herein the results obtained with the continuous and ultrafast synthesis of monodisperse superparamagnetic ferrite nanoparticles in supercritical ethanol. The advantages of a continuous flow reaction over a batch system include a better control of the experimental conditions, especially residence times, a much faster synthesis of the material (90 s) and the interest of continuous fabrication processes when considering scaling-up production of nanomaterials. In addition, the solvent could be recovered, recycled and reused.

It is known that by varying the temperature and pressure, the physico-chemical properties of supercritical fluid media can be tuned (*e.g.* density, dielectric constant, viscosity).[17,19–21,27,43] These have a direct impact on the reaction kinetics, corresponding to an enhancement of the reaction rate k in the critical region, according to the Born theory:[27] $\ln k = \ln k_0 - (\omega/RT)(1/\varepsilon - 1/\varepsilon_0)$, where ω is a constant determined in the reaction system, ε, ε_0 are the dielectric constants and k_0 is the rate constant for $\omega = \omega_0$. Furthermore, it is admitted that controlling the kinetics impacts directly the nucleation and growth of NPs. For instance, the Iversen group[28] performed *in situ* synchrotron X-ray studies on the nucleation and growth of magnetite nanoparticles in supercritical water (scH_2O). It has been demonstrated that the precursor is entirely consumed within seconds, due to high nucleation rate, therefore providing fully crystalline magnetite NPs, in agreement with others.[27] This behavior was also studied in other supercritical solvents, such as methanol (scMeOH). In comparison with scH_2O, scMeOH has a lower dielectric constant close to its critical point, resulting in the decrease of the monomer solubility and therefore a higher supersaturation, leading to smaller crystallite size.[22,44] Additionally, the Aymonier group has recently reported that supercritical alcohols play a role not only as reducing reaction media, but also as capping agents (surface modifiers) for the synthesis of cerium oxide nanocrystals.[45] In supercritical alcohols[21,22,33,34,44–46] the metal precursor is thermally decomposed inducing a high degree of supersaturation and subsequently a burst nucleation followed by crystal growth resulting in narrow particle size distributions. When the reaction is performed with preheated reagent streams in a continuous way, the nucleation generally occurs at the mixing point, while further crystal growth happens in the reactor.[21] In our system (Fig. 1), the reagent streams (precursor and surfactant solutions) meet at the mixing point at room temperature. Therefore, we can assume that the nucleation is slightly delayed and starts only in the heated supercritical zone (260 °C) followed by a fast growth and surfactant capping.

Two aspects of the process were investigated: first, the preparation and comparison of iron oxide NPs obtained from two different types of precursors: (i) a metal salt Fe(III) nitrate, (A) and (ii) a metal precursor Fe(III) acetylacetonate, (B), both being *in situ* functionalized. Second, the synthesis of $MnFe_2O_4$ NPs, by adding the Mn(II) acetate precursor to $Fe(acac)_3$ in the corresponding molar ratio, by specifically focusing on the comparison between the *in situ* (C) and *ex situ* (D) NP surface functionalization.

Structural and morphological characterization

The powder X-ray diffraction (XRD) patterns of ferrite (MFe_2O_4, M = Mn, Fe) NPs are presented in Fig. 2. Since the typical maghemite (ICDD PDF039-1346) and magnetite (ICDD PDF019-0629) reflection peaks are very close to each other, and that our materials exhibit broad reflection peaks, a clear distinction cannot be made between the two inverse spinel phases. However, the cell lattice parameters obtained from the MAUD refinement of the iron oxide NPs (Fig. 2a) were found to be

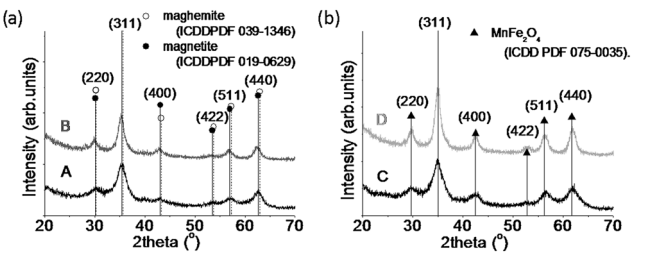

Fig. 2 X-ray patterns of ferrite nanoparticles synthesized in continuous scEtOH: (a) Fe_3O_4 NPs synthesized using $Fe(NO_3)_3$ (A) and $Fe(acac)_3$ (B); (b) $MnFe_2O_4$ NPs prepared with *in situ* (C) and *ex situ* (D) functionalization. All patterns are in agreement with the corresponding bulk materials.

8.387 ± 0.005 Å (A) and 8.400 ± 0.004 Å (B), respectively, both very close to the lattice constant of the bulk magnetite unlike the one corresponding to maghemite. We can thus conclude that our NPs consist of a mixture of maghemite and magnetite, the latter being predominant, which is consistent with supercritical ethanol generally acting as a reducing agent, as reported elsewhere.[22,26] Moreover, the phase ratio also depends on the considered metal precursor, as revealed by titration (10% of Fe^{2+} when the precursor is iron nitrate and 21% of Fe^{2+} when the precursor is iron acetylacetonate). The crystallite sizes $\langle \Phi_{XRD} \rangle$ calculated by the Scherrer equation, corresponding to the highest intensity reflection peak (311) of the XRD pattern, were 4.3 nm (A) and 6 nm (B), respectively. The reflection peaks of patterns C and D (Fig. 2b) were indexed with those of the cubic inverse spinel for the manganese ferrite phase with lattice parameters of 8.448 ± 0.005 Å (C) and 8.469 ± 0.002 Å (D), respectively (the lattice constant for bulk phase is 8.511 Å, ICDD PDF075-0035). The crystalline sizes of manganese ferrite calculated (by the Scherrer equation) were 3.9 nm (C) and 7.1 nm (D).

The size, polydispersity and shape of ferrite NPs were further investigated by TEM. The Figs. 3 and 4 display images of the obtained magnetic NPs. Fe_3O_4 NPs were obtained from $Fe(NO_3)_3 \cdot 9H_2O$ (A) (Fig. 3a) and $Fe(acac)_3$ (B) (Fig. 3b), respectively, in the presence of a mixture of surfactants oleic acid and oleylamine (3 : 3 : 1 to Fe^{3+}). For both materials, the mean size is similar (~5.5 nm), with an equivalent polydispersity of 27% (A) and 25% (B), respectively (Fig. 3a and b, insets), in agreement with XRD. However, one can notice difference in morphologies. The NPs synthesized from a nitrate precursor (A) present a more irregular shape compared to those from acetylacetonate (B), which are more spherical. This could result from the different nature of the metal precursor (a salt and a metal compound). The regular shape of NPs obtained from $Fe(acac)_3$ and their larger saturation magnetization value (see Fig. 6a and b) point out an improved crystallinity, likely as a consequence of a more synchronic nucleation and growth at well-defined temperatures.

The $MnFe_2O_4$ NPs (Fig. 4) were synthesized by adding the Mn(II) precursor to one of the Fe(III) precursors (in a molar ratio Mn : Fe of 1 : 2), while keeping the same reaction parameters previously detailed. Surprisingly, the synthesis of manganese ferrite using Fe(III) nitrate and Mn(II) acetate either in the presence or absence of surfactants (OAc and OAm) resulted in a very poor reaction yield compared to the pure Fe_3O_4 synthesis (A) (results not shown). This could be due to the different solubility and decomposition temperatures of the precursors[47,48] in supercritical ethanol or due to a phase segregation of the two metals. When changing the iron nitrate precursor for $Fe(acac)_3$, magnetic manganese ferrite NPs were formed. Unlike $Fe(NO_3)_3$, the $Fe(acac)_3$ precursor decomposes at an onset temperature of 186 °C (ref. 49) close to that of $Mn(ac)_2$ (192 °C),[48] this being a prerequisite for the successful synthesis of binary metal oxide nanocrystals.[49] TEM images of the as-prepared *in situ* and *ex situ* functionalized NPs are presented in Fig. 4. When the synthesis was performed in the presence of OAc (C) (Fig. 4a), very small (~3 nm) NPs were obtained, in agreement with other studies.[46,50] On the other hand, in the absence of surfactants (D) (Fig. 4b), high quality NPs with a mean size of around 7 nm and a polydispersity of ~16% could be produced. The difference in size of NPs functionalized *in situ* and *ex situ* indicates that the surfactants can interfere with the nucleation and growth of NPs as reported for other systems.[46,50]

The surface chemistry of the prepared ferrite NPs was analyzed by dynamic light scattering (DLS) and thermogravimetry analysis (TGA) (Fig. 5). The *in situ* and *ex situ* functionalization affects not only the size of the produced NPs, but also their colloidal stability. The monodispersity and time stability of the hexane colloidal dispersions were monitored by DLS measurements as size distribution by volume% (Fig. 5a and c). The ferrite NPs synthesized in the presence of surfactant (B) (Fig. 5a) are more stable over time; the values of the maximum peak position ($\langle \Phi_{HYD} \rangle$) for the as-prepared material and after six months of storage are found to be very close: 16 nm and 18 nm, respectively. As it was reported for iron oxide NP synthesis by the thermal decomposition route,[51] the surfactant oleic acid covalently binds to the NP surface, ensuring a stable protective shell around the magnetic core. This chemisorbed organic shell can be detected by TGA through a weight loss at high temperature. Although the TGA curve (Fig. 5b) seems to show only a

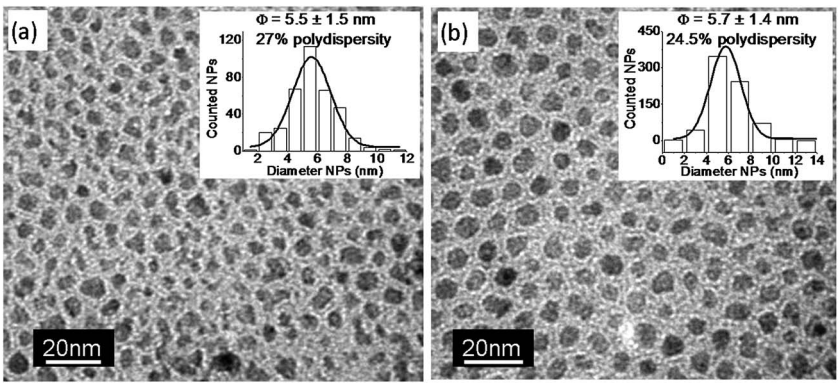

Fig. 3 Transmission electron microscopy (TEM) images of Fe_3O_4 NPs synthesized from $Fe(NO_3)_3$ (a) and $Fe(acac)_3$ (b) precursors. The size distributions were fitted to a Gaussian function and are presented as insets.

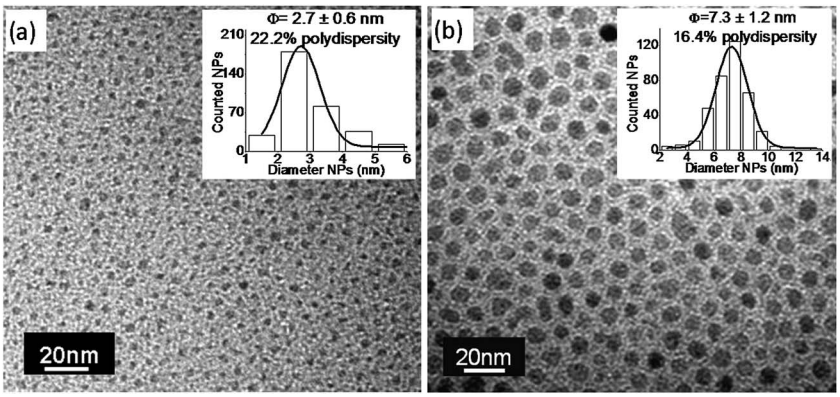

Fig. 4 Transmission electron microscopy (TEM) images of manganese ferrite NPs synthesized in the presence (a) and absence (b) of OAc. The Gaussian size distributions are shown as insets.

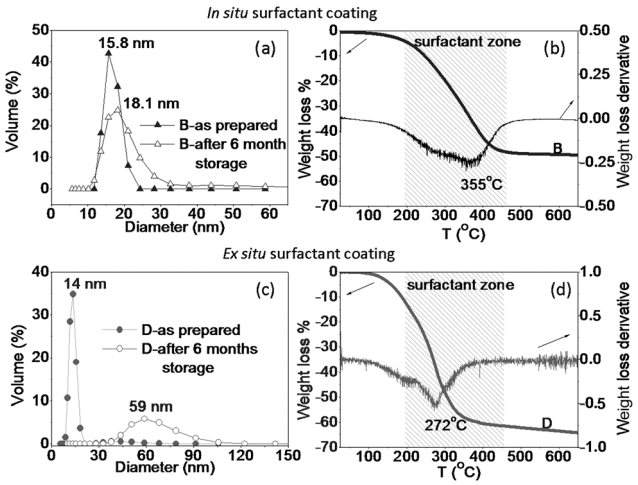

Fig. 5 Surface chemistry analysis of *in situ* and *ex situ* surfactant coated nanoparticles: dynamic light scattering measurements on hexane colloidal dispersion (a and c) and thermogravimetry analyses (b and d).

single weight loss step, the derivative function exhibits a very broad peak with a global minimum at ~355 °C and a weak local minimum at ~265 °C. The peak at 355 °C suggests the presence of chemisorbed surfactants on the NP surface, while the peak at 265 °C is related to the physisorbed surfactant shell, being present in much less quantity.[51] Different results were found when the magnetic NPs were *ex situ* functionalized with OAc (D). The weight loss derivative (Fig. 5d) shows two peaks at much lower temperatures (~200 °C and ~272 °C) suggesting the presence of both free and physisorbed surfactants. It can be assumed that no covalent bonds formed between the oleic acid and the iron oxide NP surface, since the *ex situ* coating was carried out at a low temperature (~50 °C). This physisorbed capping shell was found to be useful in preventing massive NP aggregation and thus avoiding their flocculation, although it was not strong enough to completely prevent NP agglomeration over time.[51] Indeed, aggregate formation was significant after six months of liquid storage, as confirmed by the shift of the maximum peak position monitored by DLS measurements (Fig. 5c).

Magnetic characterization

For most applications using magnetic NPs, superparamagnetic behaviour at room temperature is required since they can provide a large response at low magnetic field while providing no response in its absence. The magnetic properties of ferrite NPs were evaluated by (i) magnetization *vs.* magnetic field measurements at 300 K and 5 K and (ii) zero-field-cooled (ZFC) and field-cooled (FC) temperature dependent magnetization curves (Fig. 6). Fig. 6a and c show typical magnetization curves for superparamagnetic NPs with neither a hysteresis loop nor remanent magnetization nor coercivity at room temperature. Superparamagnetism is furthermore confirmed by the ZFC-FC magnetization curves (Fig. 6b and d) with measured blocking temperatures (T_B) of 42 K (A), 52 K (B) and 58 K (D), respectively. The absence of T_B for material C reveals the presence of a predominant paramagnetic component due to the very small NP size or even to some unreacted precursors not completely removed from the final material. It is worth noting the high

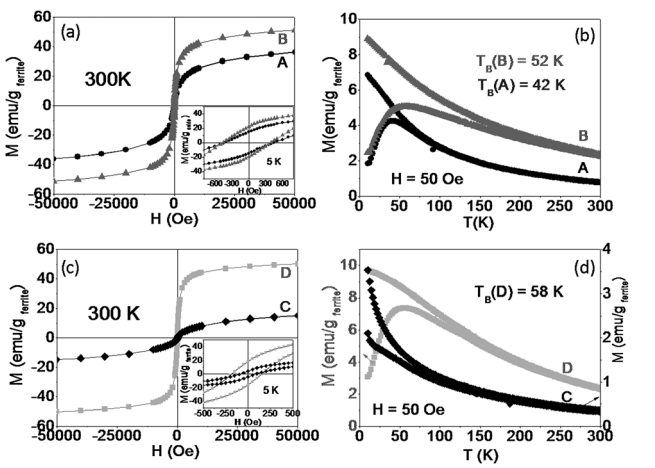

Fig. 6 Magnetometry data. Hysteresis loops at 300 K for the Fe_3O_4 (a) and $MnFe_2O_4$ (c) nanoparticles. The insets (a and c) correspond to $M(H)$ at 5 K showing coercivity. The ZFC-FC curves show the blocking temperatures (T_B) for Fe_3O_4 (b) and $MnFe_2O_4$ (d).

magnetization saturation values for system B (approx. 50 emu/g Fe_3O_4), which points out the higher crystallinity of these NPs compared to system A, presenting a similar mean particle size but with more irregular shapes. A high value of the saturation magnetization was equally achieved for system D.

Conclusions

By using metal precursors (metal acetate or acetylacetonate) at a temperature of 260 °C and at a pressure of 20 MPa in a continuous supercritical ethanol process, high quality superparamagnetic ferrite NPs (<10 nm) could be produced within an extremely short residence time (90 s). *In situ* and *ex situ* functionalization produced stable NP colloidal dispersions with different time stabilities depending on the functionalization strategy. Considering its environmentally friendly, effective and good product quality features, the continuous supercritical ethanol synthesis process appears to be a promising green technology for the future implementation of industrial production of magnetic NPs.

Acknowledgements

This work was partially funded by the Spanish Government (MAT2012-35324, CONSOLIDER-Nanoselect-CSD2007-00041) and the Generalitat de Catalunya (2009SGR203). We also acknowledge the Conseil Régional d'Aquitaine (France) for financial support.

References

1 N. Lee and T. Hyeon, *Chem. Soc. Rev.*, 2012, **41**, 2575–2589.
2 S. Singamaneni, V. N. Bliznyuk, C. Binek and E. Y. Tsymbal, *J. Mater. Chem.*, 2011, **21**, 16819–16845.
3 J. S. Beveridge, J. R. Stephens and M. E. Williams, *Annu. Rev. Anal. Chem.*, 2011, **4**, 251–273.
4 *Inorganic Nanoparticles: Synthesis, Applications and Perspectives*, ed. C. Altavilla and E. Ciliberto, CRS Press, Boca Raton, 2011.
5 E. Taboada, E. Rodríguez, A. Roig, J. Oro, A. Roch and R. N. Muller, *Langmuir*, 2007, **23**, 4583–4588.
6 *Magnetic Nanoparticles*, ed. S. P. Gubin, WILEY-VCH, Weinheim, 2009.
7 J. M. Caicedo, O. Pascu, M. López-García, V. Canalejas, A. Blanco, C. López, J. Fontcuberta, A. Roig and G. Herranz, *ACS Nano*, 2011, **5**(4), 2957–2963.
8 O. Pascu, J. M. Caicedo, M. López-García, V. Canalejas, A. Blanco, C. López, J. Arbiol, J. Fontcuberta, A. Roig and G. Herranz, *Nanoscale*, 2011, **3**, 4811–4816.
9 X. Sun, D. Ho, L.-M. Lacroix, J. Q. Xiao and S. Sun, *IEEE Transactions on NanoBioscience*, 2012, **11**(1), 46–53.
10 L. Fan, Y. Zhang, C. Luo, F. Lu, H. Qiu and M. Sun, *Int. J. Biol. Macromol.*, 2012, **50**, 444–450.
11 Y. Wang, R. Cheng, Z. Wen and L. Zhao, *Eur. J. Inorg. Chem.*, 2011, 2942–2947.
12 S. Sun, H. Zeng, D. B. Robinson, S. Raoux, P. M. Rice, S. X. Wang and G. Li, *J. Am. Chem. Soc.*, 2004, **126**, 273–279.
13 V. Polshettiwar, R. Luque, A. Fihri, H. Zhu, M. Bouhrara and J.-M. Basset, *Chem. Rev.*, 2011, **111**, 3036–3075.
14 E. M. Siedlecka, M. Czerwicka, J. Neumann, P. Stepnowski, J. F. Fernández and J. Thöming, in *Ionic Liquids: Theory, Properties, New Approaches*, ed. A. Kokorin, InTech, Rijeka, 2011, ch. 28, pp. 701–723.
15 J.-W. Moon, C. J. Rawn, A. J. Rondinone, L. J. Love, Y. Roh, S. M. Everett, R. J. Lauf and T. J. Phelps, *J. Ind. Microbiol. Biotechnol.*, 2010, **37**, 1023–1031.
16 T. Adschiri, Y. W. Lee, M. Goto and S. Takami, *Green Chem.*, 2011, **13**, 1380–1390.
17 C. Aymonier, A. Loppinet-Serani, H. Reveron, Y. Garrabos and F. Cansell, *J. Supercrit. Fluids*, 2006, **38**, 242–251.
18 U. T. Lam, R. Mammucari, K. Suzuki and N. R. Foster, *Ind. Eng. Chem. Res.*, 2008, **47**, 599–614.
19 E. Reverchon and R. Adamia, *J. Supercrit. Fluids*, 2006, **37**, 1–2.
20 R. Sui and P. Charpentier, *Chem. Rev.*, 2012, **112**(6), 3057–3082.
21 F. Cansell and C. Aymonier, *J. Supercrit. Fluids*, 2009, **47**, 508–516.
22 B. Veriansyah, J.-D. Kim, B. K. Min and J. Kim, *Mater. Lett.*, 2010, **64**, 2197–2200.
23 S. K. Pahari, T. Adschiri and A. B. Panda, *J. Mater. Chem.*, 2011, **21**(28), 10377–10383.
24 J. Becker, P. Hald, M. Bremholm, J. S. Pedersen, J. Chevallier, S. B. Iversen and B. B. Iversen, *ACS Nano*, 2008, **2**(5), 1058–1068.
25 E. Taboada, R. Solanas, E. Rodríguez, R. Weissleder and A. Roig, *Adv. Funct. Mater.*, 2009, **19**, 2319–2324.
26 Z. Li, J. F. Godsell, J. P. O'Byrne, N. Petkov, M. A. Morris, S. Roy and J. D. Holmes, *J. Am. Chem. Soc.*, 2010, **132**, 12540–12541.
27 T. Adschiri, Y. Hakuta and K. Arai, *Ind. Eng. Chem. Res.*, 2000, **39**, 4901–4907.
28 M. Bremholm, M. Felicissimo and B. B. Iversen, *Angew. Chem., Int. Ed.*, 2009, **48**, 4788–4791.
29 C. Xu and A. S. Teja, *J. Supercrit. Fluids*, 2006, **39**, 135–141.
30 D. Zhao, X. Wu, H. Guan and E. Han, *J. Supercrit. Fluids*, 2007, **42**, 226–233.
31 S. Marre, F. Cansell and C. Aymonier, *Nanotechnology*, 2006, **17**, 4594–4599.
32 K. Matsuyama, K. Mishima, T. Kato and K. Ohara, *Ind. Eng. Chem. Res.*, 2010, **49**, 8510–8517.
33 Y. Roig, S. Marre, T. Cardinal and C. Aymonier, *Angew. Chem., Int. Ed.*, 2011, **50**, 12071–12074.
34 D. Rangappa, K. Sone, M. Ichihara, T. Kudo and I. Honma, *Chem. Commun.*, 2010, **46**, 7548–7550.
35 J. F. Bocquet, K. Chhor and C. Pommier, *Mater. Chem. Phys.*, 1999, **57**, 273–280.
36 H. Reveron, C. Aymonier, A. Loppinet-Serani, C. Elissalde, M. Maglione and F. Cansell, *Nanotechnology*, 2005, **16**, 1137–1143.

37 H. Reveron, C. Elissalde, C. Aymonier, O. Bidault, M. Maglione and F. Cansell, *J. Nanosci. Nanotechnol.*, 2005, **5**, 1741–1744.
38 P. Hald, J. Becker, M. Bremholm, J. S. Pedersen, J. Chevallier, S. B. Iversen and B. B. Iversen, *J. Solid State Chem.*, 2006, **179**, 2674–2680.
39 S. Marre, J. Park, J. Rempel, J. Guan, M. G. Bawendi and K. F. Jensen, *Adv. Mater.*, 2008, **20**, 4830–4834.
40 S. Marre, J. Baek, J. Park, M. G. Bawendi and K. F. Jensen, *JALA*, 2009, **14**, 267–273.
41 J. D. Pritchand, *in HPA Compedium of Chemical Hazards Methanol*, CRCE HQ, Health Protection Agency, version 3, 2011.
42 S. Moisan, J.-D. Marty, F. Cansell and C. Aymonier, *Chem. Commun.*, 2008, 1428–1430.
43 N. Ventosa, in *Supercritical Fluids & Materials*, ed. C. Aymonier, F. Cansell and O. Fouassier, Arcachon, 2007, pp. 167–179.
44 B. Veriansyah, H. Park, J.-D. Kim, B. K. Min, Y. H. Shin, Y.-W. Lee and J. Kim, *J. Supercrit. Fluids*, 2009, **50**, 283–291.
45 C. Slostowski, S. Marre, O. Badot, T. Toupance and C. Aymonier, *Langmuir*, 2012, **28**, 16656–16663.
46 J. Kim, D. Kim, B. Veriansyah, J. W. Kang and J. D. Kim, *Mater. Lett.*, 2009, **63**(21), 1880–1882.
47 K. Wieczorek-Ciurowa and A. J. Kozak, *J. Therm. Anal. Calorim.*, 1999, **58**, 647–651.
48 W. Ciesielski and P. Tomasik, *Thermochim. Acta*, 2003, **403**, 161–171.
49 Q. Song, Y. Ding, L. Z. Wang and Z. Zhang, *Chem. Mater.*, 2007, **19**(19), 4633–4638.
50 B. Veriansyah, H. Park, J.-D. Kim, B. K. Min, Y. H. Shin, Y.-W. Lee and J. Kim, *J. Supercrit. Fluids*, 2010, **52**, 76–83.
51 O. Pascu, E. Carenza, M. Gich, S. Estradé, F. Peiró, G. Herranz and A. Roig, *J. Phys. Chem. C*, 2012, **116**, 15108–15116.